IOP Publishing Journal of Physics D: Applied Physics

J. Phys. D: Appl. Phys. **49** (2016) 075302 (10pp) doi:10.1088/0022-3727/49/7/075302

Size-dependent complex dielectric function of Ni, Mo, W, Pb, Zn and Na nanoparticles. Application to sizing

David Muñetón Arboleda[1], Jesica M J Santillán[1,2], Luis J Mendoza Herrera[1], Diego Muraca[3], Daniel C Schinca[1,4] and Lucía B Scaffardi[1,4]

[1] Centro de Investigaciones Ópticas (CIOp), (CONICET La Plata—CIC), La Plata, Argentina
[2] Departamento de Química, Facultad de Ciencias Exactas y Naturales, UNCa, Catamarca, Argentina
[3] Instituto de Física 'Gleb Wataghin' (IFGW), Universidade Estadual de Campinas, Brazil
[4] Departamento de Ciencias Básicas, Facultad de Ingeniería, UNLP, Argentina

E-mail: lucias@ciop.unlp.edu.ar

Received 23 September 2015, revised 23 November 2015
Accepted for publication 17 December 2015
Published 14 January 2016

Abstract

This work determines the size dependent metal nanoparticle (NP) dielectric function from a 'top-down' approach using the bulk experimental refractive index as a starting point. Free-electron damping constant (γ_{free}) and plasma frequency (ω_p) parameters in the Drude model are calculated for nickel (Ni), molybdenum (Mo), tungsten (W), lead (Pb), zinc (Zn) and sodium (Na) using a method developed in our group. Determined γ_{free} and ω_p parameters allow to develop an expression that improves the precision in reproducing the discrete metal bulk dielectric function in a wide wavelength range (UV-FIR). The bulk dielectric function is modified for describing the nanometric case by adding size corrective terms for free and bound electrons contributions. As an application of this study we characterize Ni spherical NPs synthesized by ultrafast laser ablation of a solid target in water. Using Mie theory together with the size-dependent dielectric function, we theoretically reproduce its experimental extinction spectrum. From this fitting, composition and size distribution of the particles in the colloidal suspension may be derived. Transmission electron microscopy (TEM) results agree with the sizes and structure derived from optical extinction spectroscopy (OES).

Keywords: metal nanoparticles, dielectric function, size dependent optical properties

(Some figures may appear in colour only in the online journal)

1. Introduction

Metal nanostructures, and specifically NPs, have received increasing attention in several fields of basic and applied science, owing to their new and interesting properties compared with bulk material. The tuning of these new properties by controlling the nanostructure of materials has been shown to be suitable in particular applications [1, 2]. In the last decades, scientific interest has been focused on the generation and analysis of NPs of noble metals for their characteristic optical, electrical and biological properties. However, few works are devoted to exploring metals out of this group which have specific applications in different areas of science and technology. For example, Ni, Mo, W, Pb, Zn and Na metal NPs present attractive applications in the areas of biomedicine [3–11], materials science [7, 12], agronomy [13, 14], catalysis [15], information storage [15], superparamagnetism [16, 17], sensors [18], electronic devices [5], solar cells [19], hydrogen production [20], among others.

It is well known that when the size of metal objects approaches the nanometer range, new properties in the material can be observed, and optical properties are no exception [21]. Thus, various efforts are focused on developing a quantitative and qualitative modeling to describe such changes. Many of these studies are based on a top-down approach, relying on corrections added to models describing the properties of

metals in bulk. With this kind of theoretical construction, studies of radiation-matter interaction at the nanometer scale may be carried out without the need for entering in quantum mechanics calculations. In order to make an appropriate correction of a macroscopic model, adequate determination of specific parameters is needed.

The simplest model to study optical properties of bulk metals based on its dielectric function is the so called Drude model. It is based on the interpretation of a metal as an array of fixed positive ions embedded in a 'sea' of essentially free electrons. When an electromagnetic wave interacts with the metal, the electrons are forced to oscillate by the incoming wave. The equation of a forced oscillator contains two parameters: the damping constant of free electrons γ_{free} and the plasma frequency ω_{p} [22].

These parameters are usually determined based on the mathematical approximation $\omega \gg \gamma_{\text{free}}$, which allows obtaining a linear relation between the real part of the dielectric function ($\varepsilon'(\omega)$) and λ^2, from which ω_p can be derived. However, the approximation restricts the frequency values to the UV-deep UV region [23–25], where the Drude model may not be valid since, for this wavelength range, bound electron transition must be considered.

In this work we determine for the first time the Drude model parameters γ_{free} and ω_{p} for Ni, Mo, W, Pb, Zn and Na employing a method developed by Mendoza Herrera *et al* [26], which lifts the restriction $\omega \gg \gamma_{\text{free}}$. It will be shown that the so obtained γ_{free} and ω_{p} allow a much more accurate fitting of the experimental bulk dielectric function discrete values in a wider wavelength range, beyond the visible and extending to the FIR depending of the metal. The high reliability of the obtained continuous dielectric function enhances a much better knowledge of the bulk optical properties of these metals, which is the basis for calculating the optical response in the nanometric scale.

For nanosized metals, certain considerations must be taken into account. For the case of spherical NPs under 20 nm radii, the complex dielectric function becomes size dependent through corrections introduced specifically into γ_{free} and considering bound-electron effects. In this way, the dielectric function can be written as the sum of two contributions, one corresponding to free electrons (intraband transitions) and the other to bound electrons (interband transitions). Thus, taking into account the values of the Drude parameters determined in this work, we calculate the size-dependent complex dielectric function for each of the studied metals, considering the size corrections on free and bound electron contributions.

Finally, based on the knowledge of the dielectric function, we show an application to the theoretical calculation of Ni extinction spectra for different structures and configurations using Mie theory. These calculations allow fitting the experimental optical extinction spectrum of a colloidal suspension of Ni NPs generated by ultrafast laser ablation in water, using the size distribution as the fitting parameter. Inspection of TEM images of the generated sample assures the spherical NPs shape and allows observing structures and sizes that agree with those derived from OES.

2. Determination of γ_{free} and ω_{p} and theoretical analysis of size-dependent metal dielectric function

2.1. Determination of γ_{free} and ω_{p}

Optical properties of materials may be alternatively described by the complex refractive index $(n + \mathrm{i}k)$ or the complex dielectric function $(\varepsilon' + \mathrm{i}\varepsilon'')$, which are related to each other through the expressions $\varepsilon' = n^2 - k^2$ and $\varepsilon'' = 2nk$. In the Drude model, the complex dielectric function for free electrons is written as [22, 27, 28]:

$$\varepsilon_{\text{free}}(\omega) = 1 - \frac{\omega_{\text{p}}^2}{\omega^2 + \mathrm{i}\omega\gamma_{\text{free}}} = 1 - \frac{\omega_{\text{p}}^2}{\omega^2 + \gamma_{\text{free}}^2} + i\frac{\omega_{\text{p}}^2\gamma_{\text{free}}}{\omega\,(\omega^2 + \gamma_{\text{free}}^2)} \quad (1)$$

where ω_{p} is, as stated previously, the plasma frequency and γ_{free} is the damping constant of the electron oscillatory movement, that is due to different types of collisions: electron-electron, electron-ion and electron-phonon. These processes are characterized by the mean time between two successive collisions and are considered altogether in the γ_{free} value, since they cannot be specifically separated within the framework of the model.

For low frequencies (large wavelengths), Drude model describes with good accuracy the dielectric function for metals. Thus, considering the real and imaginary parts of the equation (1), two independent linear relationships may be derived and expressed as [26]:

$$f_1(\omega) \equiv \omega\varepsilon''(\omega) = \gamma_{\text{free}}(1 - \varepsilon'(\omega)) \quad (2)$$

$$f_2(\omega) \equiv \omega^2\left[(\varepsilon''(\omega))^2 + (1 - \varepsilon'(\omega))^2\right] = \omega_{\text{p}}^2(1 - \varepsilon'(\omega)) \quad (3)$$

If $f_1(\omega)$ and $f_2(\omega)$ are plotted against $(1 - \varepsilon'(\omega))$, a linear relationship should be obtained. Values of $\varepsilon(\omega)$ can be derived from the experimental complex refractive index data for Ni, Mo, W, Pb, Zn and Na taken from the literature [29–33]. These authors report measurements of the refractive index in a given range of wavelength for each metal (670 nm–80 000 nm for Ni [29], 670 nm–80 000 nm for Mo [30], 206 nm–12 400 nm for W [31], 670 nm–6670 nm for Pb [29], 1230 nm–70000 nm for Zn [32] and 326 nm–2070 nm for Na [33]). Therefore, when these data are used in equations (2) and (3), it is possible to fit $f_1(\omega)$ and $f_2(\omega)$ with a linear regression in the region of large wavelengths where the Drude model is dominant. From their slopes, γ_{free} and ω_{p} are determined.

Figure 1 shows the plots of $f_1(\omega)$ and $f_2(\omega)$ as a function of $(1 - \varepsilon'(\omega))$ for the above mentioned metals. The filled circles correspond to data obtained from equations(2) and (3), and full line represents the linear fit (with zero ordinate intercept) only for those data that satisfy the Drude model. In each panel, dashed lines are the extrapolation of the full lines to the origin. It can be seen that these lines miss fitting many data points, suggesting a frequency range where Drude model is not satisfied. This is due to the influence of interband transitions which were not taken into account to describe the dielectric function.

Table 1 shows the ω_{p} and γ_{free} parameters determined for the first time in this work for the six analyzed metals, together with the values given by other authors for comparative purposes.

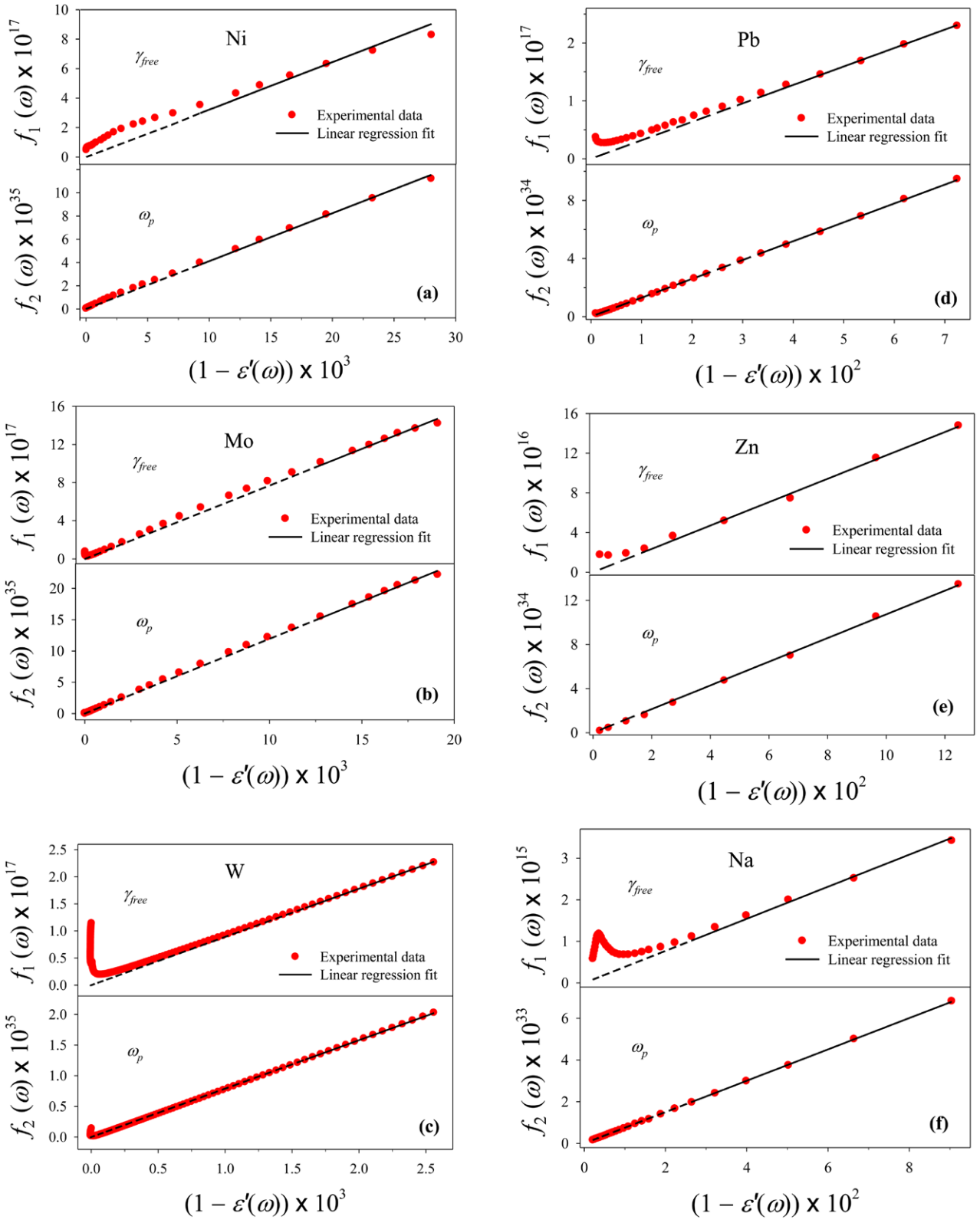

Figure 1. Plot of $f_1(\omega)$ and $f_2(\omega)$ as a function of $(1-\varepsilon'(\omega))$ for: (a) Ni, (b) Mo, (c) W, (d) Pb, (e) Zn and (f) Na. Full circles represents the functions calculated with experimental data. Full line represents the linear regressions where the dielectric function can be described by the Drude model. Dashed lines indicate the extrapolation of the full line to the origin. The slopes of the linear fits allow determining the values of γ_{free} and ω_p. Experimental data of the complex refractive index are taken from [29] for Ni and Pb [30], for Mo [31], for W [32], for Zn and [33] for Na.

Table 1. ω_p and γ_{free} parameters determined in this work together with those calculated by other authors.

Metal	ω_p [1/s] $\times 10^{15}$	γ_{free}[1/s] $\times 10^{13}$	References
Ni	6.408 ± 0.121	3.160 ± 0.245	(this work)
	7.427	3.355	[29]
Mo	10.929 ± 0.302	7.693 ± 0.551	(this work)
	11.347	7.766	[30]
W	8.887 ± 0.019	8.900 ± 0.074	(this work)
	20.085	9.723	[31]
Pb	11.413 ± 0.214	31.712 ± 0.992	(this work)
	11.197	22.148	[30]
Zn	10.360 ± 0.132	11.778 ± 0.493	(this work)
	14.4	10.8	[32, 34]
Na	8.669 ± 0.037	3.868 ± 0.173	(this work)
	8.569	4.193	[33, 35]

The errors in their determination listed in the Table correspond to the root-mean-square deviation (RMSD) of the least squares fit. As it is known, RMSD is a good measure of precision. The percentage errors derived from RMSD are 0.2%–2.7% for ω_p and 0.8%–8% for γ_{free}, thus showing a greater precision in our determination. The parameters values and their RMSD are given with the same number of decimal places as those used by other author for comparison purposes. Such precision is indeed needed for a reliable reproduction of the dielectric function.

The obtained values of ω_p and γ_{free} may be introduced in equation (1) to fit the experimental complex dielectric function for each metal. Figure 2 shows the real and imaginary parts of the experimental bulk dielectric function (hollow circles) for Ni, Mo, W, Pb, Zn and Na. Dashed lines represent the complex dielectric function calculated with our values of ω_p and γ_{free}, while dashed-dotted lines show the dielectric function calculated with the values of these parameters reported in the literature. It can be readily seen that, for each metal, the best fit to the experimental bulk complex dielectric function values is given by the calculation performed with our parameters. The so determined function yields very reliable results even for those wavelengths for which no experimental values are given. It can also be seen the noticeable divergence for large wavelengths between theoretical calculations using ω_p and γ_{free} taken from other authors and the experimental values taken from the literature. On the other hand, the excellent agreement between experimental data and its calculated fit shown in the different panels, supports the goodness of our method for determining ω_p and γ_{free}. It is worth noting the case of W plotted in panel (c), where the inset depicts a zoom in the vertical axis to show the coincidence between the experimental values and the theoretical fit determined with our method.

As mentioned above, the Drude model reproduces with good accuracy the experimental bulk complex dielectric function for large wavelengths where contribution of free electrons is dominant. However, for shorter wavelengths, the model fails to describe the behavior of dielectric function, since *d-sp* interband transitions of bound electrons are not taken into account. Besides, when the size of the NPs decreases to a few tens of nanometers, it is necessary to introduce a size-dependent term in the expression of the complex dielectric function both for free and bound electron contributions.

2.2. Theoretical analysis of size-dependent dielectric function

The expression of the metal complex dielectric function in the nanometric scale is not trivial. Several theoretical approaches such as the jellium model or the quantum-chemistry model [36, 37] are based on the quantum behavior of electrons in a solid and build the dielectric function in a 'bottom-up' direction. This work uses the 'top-down' approach to describe the dielectric function taking into account a suitable and physically meaningful modification to extend the semi-classical description for sizes down to a few nanometers [38–40].

In general, the experimental bulk complex dielectric function ($\varepsilon_{bulk}(\omega)$) may be decomposed into two contributions: a free electrons term and a bound electrons term. Since the function is additive, it can be written as:

$$\varepsilon_{bulk}(\omega) = \varepsilon_{free}(\omega) + \varepsilon_{bound}(\omega) = \varepsilon'(\omega) + i\varepsilon''(\omega) \quad (4)$$

Free electrons contribution may be suitably described by Drude model as we mentioned above (equation (1)), while the bound electrons contribution can be written taking into account interband transitions. Considering equations (1) and (4), the bound electrons contribution to the dielectric function can be expressed as:

$$\varepsilon_{bound}(\omega) = \varepsilon_{bulk}(\omega) - \left(1 - \frac{\omega_p^2}{\omega^2 + i\gamma_{free}\omega}\right) \quad (5)$$

When the radius of the metal NPs is smaller than the mean free path of the conduction electrons in the bulk metal, collisions with the particle's boundary become important. Therefore, the free electrons term must be modified to account for an increase in the damping constant due to these additional collisions. Under the assumption that the electrons are diffusely reflected at the boundary, a size-dependent expression for the damping constant is introduced in the form $\gamma_{size}(R) = \gamma_{free} + C\frac{v_F}{R}$ [22, 24]. Here, v_F is the electron velocity at the Fermi surface, R is the radius of the particle and C is a constant that depends on the metal characteristics and includes details of the scattering processes inside the particle. Thus, the size corrected complex dielectric function of free electrons contribution given by equation (1) can be now expressed as:

$$\varepsilon_{free\text{-}size}(\omega, R) = 1 - \frac{\omega_p^2}{\omega^2 + i\omega\gamma_{free} + i\omega C\frac{v_F}{R}} \quad (6)$$

Comparing equation (6) with equation (1), the above expression may be looked at from a different point of view: the size-dependent free electron dielectric function can be written as the sum of the experimental bulk dielectric function plus a size corrective term in the form:

$$\varepsilon_{free\text{-}size}(\omega, R) = \varepsilon_{free}(\omega) + \delta\varepsilon_{free}(\omega, R) \quad (7)$$

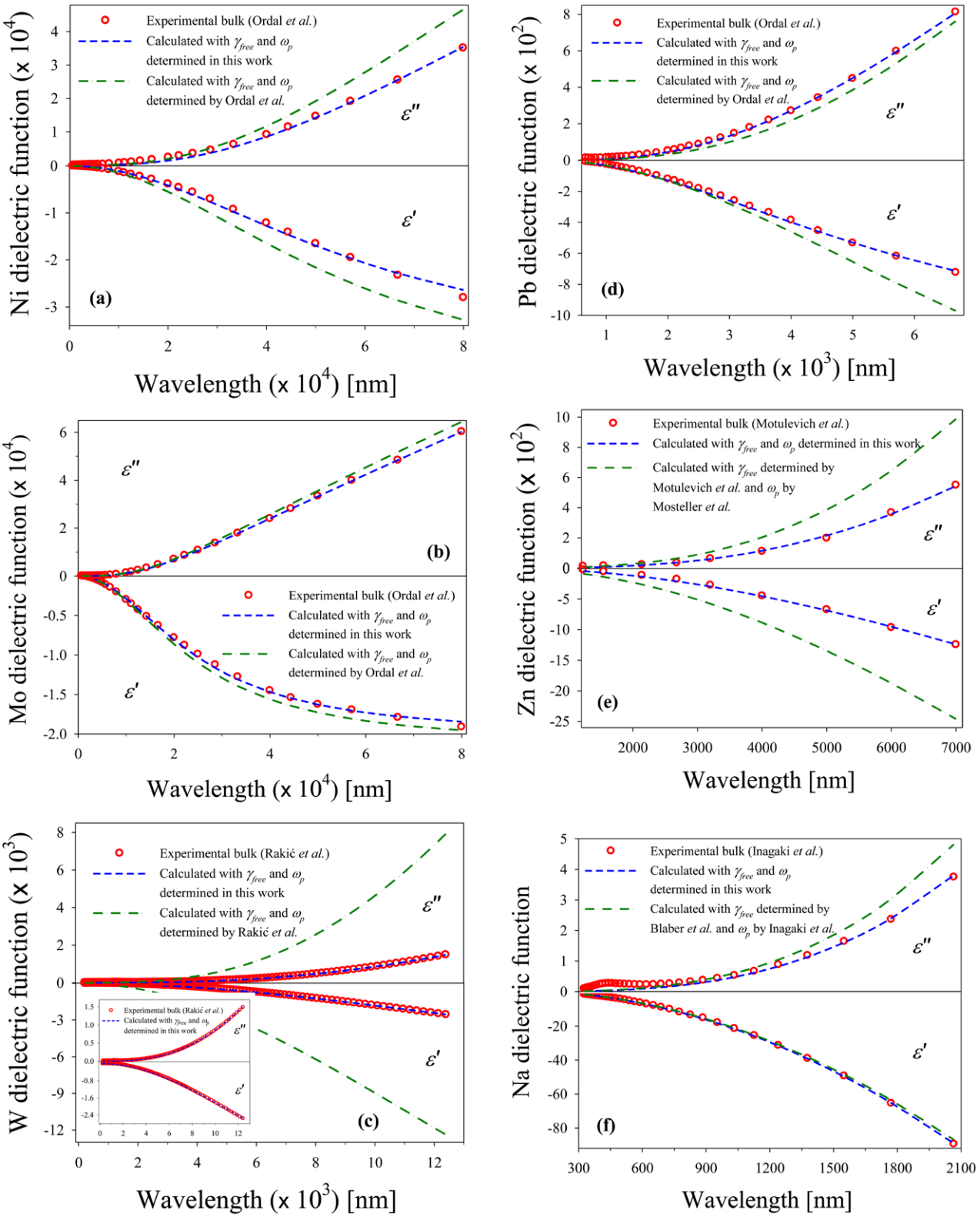

Figure 2. Experimental and theoretical bulk complex dielectric function for: (a) Ni, (b) Mo, (c) W, (d) Pb, (e) Zn and (f) Na. Hollow circles represent the real and imaginary parts of experimental bulk dielectric function. Dashed lines show the fit to the experimental complex dielectric function calculated using equation (1) and our values of ω_p and γ_{free}. Dashed-dot lines represent the same fit performed with the parameters reported by other authors (see table 1). The inset of panel (c) shows a zoom of the experimental complex dielectric function and the fit calculated from our values for a best observation.

where $\delta\varepsilon_{\text{free}}(\omega, R)$ can be determined from the last expression as:

$$\delta\varepsilon_{\text{free}}(\omega, R) = \omega_p^2\left(\frac{1}{\omega^2 + \mathrm{i}\omega\,\gamma_{\text{free}}} - \frac{1}{\omega^2 + \mathrm{i}\omega\,\gamma_{\text{free}} + \mathrm{i}\omega C\frac{v_F}{R}}\right) \quad (8)$$

On the other hand, when the particle size gets even smaller, the number of atoms in the particle decreases, generating a larger energy level separation and likewise a minor density of states. Therefore, to account for this decrease, an appropriate exponential mathematical expression $(1 - \mathrm{e}^{-(R/R_o)})$ is included in the bound electron contribution [38], obtaining the following expression:

$$\varepsilon_{\text{bound-size}}(\omega, R) = \varepsilon_{\text{bound}}(\omega) - \mathrm{e}^{-\left(\frac{R}{R_o}\right)}\varepsilon_{\text{bound}}(\omega) \quad (9)$$

where R_o is a factor that represents the range for which the density of states can be considered to reach 67% of the bulk value.

Similarly to the case of free electrons contribution, we may write the size corrected dielectric function of bound electrons contribution as the sum of the bulk bound electrons contribution plus a size corrective term:

$$\varepsilon_{\text{bound-size}}(\omega, R) = \varepsilon_{\text{bound}}(\omega) + \delta\varepsilon_{\text{bound}}(\omega, R) \quad (10)$$

Comparing equations (9) and (10) and using equation (5) we can determinate $\delta\varepsilon_{\text{bound}}(\omega, R)$ as:

$$\delta\varepsilon_{\text{bound}}(\omega, R) = -\mathrm{e}^{-\left(\frac{R}{R_o}\right)}\left(\varepsilon_{\text{bulk}}(\omega) - 1 + \frac{\omega_p^2}{\omega^2 + \mathrm{i}\omega\gamma_{\text{free}}}\right) \quad (11)$$

Extending the concept described in equation (4) for bulk, to the case of small NPs, the general expression for size dependent dielectric function can be written as:

$$\varepsilon_{\text{size}}(\omega, R) = \varepsilon_{\text{free-size}}(\omega, R) + \varepsilon_{\text{bound-size}}(\omega, R) \quad (12)$$

So, taking into account equations (4), (7) and (10), a new expression for $\varepsilon_{\text{size}}(\omega, R)$ can be rewritten as:

$$\varepsilon_{\text{size}}(\omega, R) = \varepsilon_{\text{bulk}}(\omega) + \delta\varepsilon_{\text{free}}(\omega, R) + \delta\varepsilon_{\text{bound}}(\omega, R) \quad (13)$$

where the expressions for $\delta\varepsilon_{\text{free}}(\omega, R)$ and $\delta\varepsilon_{\text{bound}}(\omega, R)$ can be regarded now as size-dependent corrective terms to the experimental bulk complex dielectric function $\varepsilon_{\text{bulk}}(\omega)$. This last equation is a simple general expression for the size-dependent complex dielectric function that contains only three parameter: γ_{free} and ω_p (determined by the method described in section 2) and the Fermi velocity, taken from the literature.

Figure 3 shows the behavior of the real and imaginary parts of equation (13), using the experimental bulk dielectric function $\varepsilon_{\text{bulk}}(\omega)$ together with equations (8) and (11) for several sizes of Ni, Mo, W, Pb, Zn and Na NPs, in the visible range. The experimental bulk dielectric function data for metals whose wavelength does not extend to the visible range are taken from [31, 41–43].

Data of ω_p, γ_{free} and v_F used for the theoretical calculations are summarized in the tables 1 and 2, respectively. Constant C is taken as 0.8 [48] and R_o as 0.35 nm [38].

It is interesting to notice that for sizes between 2 nm and 10 nm there are noticeable differences in the real and imaginary parts of all the analyzed metals, and for radii larger than 10 nm ε' and ε'' tend asymptotically to the bulk curve.

3. OES: nickel colloidal suspension in water

An important application of the study of size-dependent dielectric function is the optical characterization for metal colloidal suspensions using OES technique. As an example, we chose Ni colloidal suspension which we synthesized by 120 fs pulse Ti:Sa laser ablation method using a 1 mm thick solid disk of high purity grade Ni immersed in milli-Q water, as described by Santillán *et al* [49]. The pulse energy used in this experiment was 100 μJ.

OES was implemented by means of a Shimadzu spectrophotometer from 250 nm to 1000 nm wavelength range. Optical absorption measurement of the colloidal suspension was performed 5 min after synthesis. This kind of measurement prevents possible NPs coalescence and allows a reliable characterization of the generated sample.

It is well known that when a Ni target is ablated in water, oxidation-reduction processes may occur [50, 51]. In this situation, it is necessary to consider the possibility of generating core-shell Ni-NiO and NiO-Ni NPs as well as hollow-Ni NPs. Thus, it is appropriate to calculate their extinction spectra, since they may show optical extinction properties different from those corresponding to Ni bare core NPs. These extinction spectra were calculated using Mie theory [22] taking into account the size-dependent metal dielectric function given by equation (13) and related (8) and (11). Values for γ_{free} and ω_p are those determined in this work (table 1).

For ferromagnetic metals, as it is the case of nickel, the complex susceptibility of monodomain magnetic NPs depend of the frequency and magnetic relaxation time (τ): $\chi(\omega) = \frac{\chi_0}{1 + \mathrm{i}\omega\,\tau}$, where χ_0 is the static field susceptibility [52]. For single domain Ni NPs, the relaxation time is in the range 10^{-2}–10^{-6} s [53], and considering that our measurements are in the visible frequencies (10^{14}–10^{15} Hz), the magnetic susceptibility $\chi(\omega)$ is close to zero, making the relative permeability is $\mu_r = 1$ and allowing to apply correctly Mie theory for non magnetic NPs in the extinction calculations.

For the general case of core-shell spherical particles with core radius R and outer radius R', the extinction cross section C_{ext} depends on the core and shell size parameters and their refractive indices [22]. Sometimes, the so called extinction coefficient, that is related to the C_{ext} through the expression $Q_{\text{ext}} = C_{\text{ext}}/\pi\,R'^2$, is used for easiness of comparison.

To compare the spectral response of NPs with the different structures and configurations mentioned above, the theoretical extinction coefficients for a Ni bare-core, Ni-NiO, NiO-Ni as well as hollow-Ni NPs immersed in water were calculated. Figure 4 shows an example of this comparison for NPs with inner radius $R = 1.2$ nm, and $R' - R = 0.6$ nm for core-shell structures. A clear shoulder near 375 nm can be observed for Ni bare core, while a plasmon peak centered at 400 nm

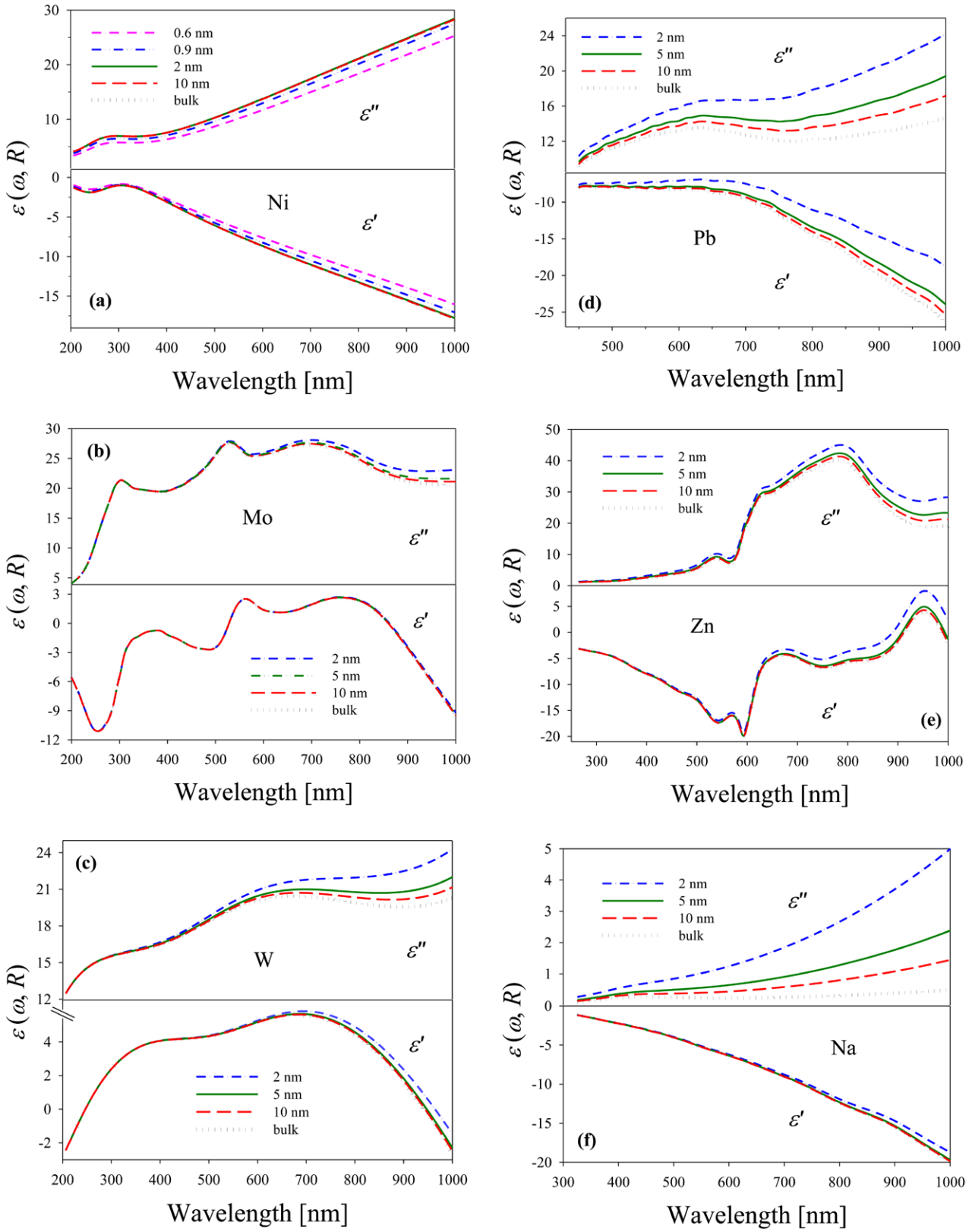

Figure 3. Theoretical values for real and imaginary parts of size-dependent dielectric function as a function of wavelength to different radii for (a) Ni, (b) Mo, (c) W, (d) Pb, (e) Zn and (f) Na. The corrected dielectric function was calculated using the equations (8), (11) and (13). Experimental data of the bulk complex dielectric function are taken from [31] for Ni and W [41], for Mo [42], for Pb [43], for Zn and [33] for Na.

Table 2. Fermi velocity for the different metals analyzed in this work.

Metal	$v_F \times 10^{14}$ [nm s^{-1}]	References
Ni	2.8	[44]
Mo	3.7	[45]
W	9.2	[46]
Pb	18.3	[47]
Zn	18.3	[47]
Na	10.7	[47]

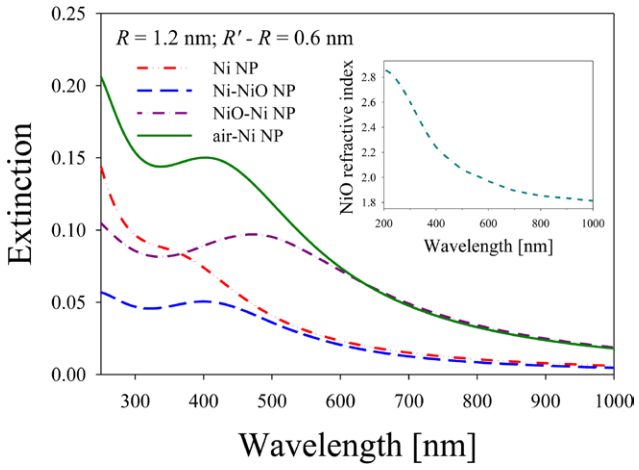

Figure 4. Theoretical extinction spectra for Ni core-shell NPs with different configurations. Inset shows the NiO refractive index reported by Mahmoud *et al* [54].

is observed for Ni-NiO NPs. For the case of NiO-Ni NPs, a plasmon peak near 470 nm can be observed, while for air-Ni NPs there is a plasmon peak near 405 nm. The inset shows the wavelength dependent refractive index for NiO, taken from the experimental data by Mahmoud *et al* [54].

Based on these results, the experimental spectrum of the Ni colloidal suspensions generated by ultrafast pulse laser ablation may be fitted. Figure 5 shows a typical experimental absorption spectrum of Ni colloidal suspension in the UV-visible-near IR range, normalized at $\lambda = 350$ nm. Full line represents the experimental data and dashed-dotted line is the theoretical fit based on a specific log-normal size distribution.

As mentioned above, when the solvent is water, some degree of oxidation is likely to occur. Structures and configurations like bare core Ni and NiO besides core-shell structures of Ni-NiO, NiO-Ni as well as air-Ni were taken into account for the fit of the Ni experimental absorption spectrum. Inset shows the total size distribution (full line) corresponding the optimum fit. Specific size distribution for air-Ni NPs (dashed-dotted line), Ni-NiO NPs (dotted line) and NiO-Ni NPs (dashed line) can also be observed. The last two size distributions include bare core Ni and NiO NPs species, respectively. It can be noticed that, each one of these species influences the extinction spectrum in specific and distinct regions in such a way that the combination of structures, configurations, sizes and relative abundances derived from optimum fit constitute a unique set of fitting parameters. For a specific species type, any small modification of size or relative abundance generates

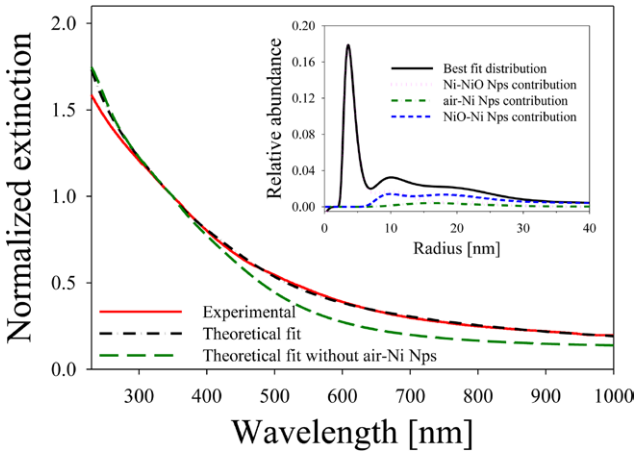

Figure 5. Comparison between experimental (full line) and theoretical (dashed-dots line) extinction spectra of Ni colloidal suspension in water. Inset shows size distribution of Ni-NiO, air-Ni and NiO-Ni NPs that fits experimental spectrum. Long dashed line represents calculated spectrum with the same distribution without considering air-Ni NPs contribution.

a noticeable change in the shape of the calculated spectrum which precludes optimum fit. It is also interesting to notice that exclusion of a specific species fails to account for large features in the experimental spectrum. Long dashed line in figure 5 is the calculated spectrum with the same distribution but without considering air-Ni NPs contribution. It can be seen that the curve misses to fit the spectrum for wavelengths larger than 390 nm. A situation similar it can be observed when the contribution of NiO-Ni NPs is not considered (not shown in figure 5).

Concerning metal hollow NPs generated by laser ablation using different pulsed lasers, these have been reported by several authors. For instance, Desarkar *et al* [55] synthesized colloidal suspensions that present Zn/ZnO hollow NPs by laser ablation with a 6 ns Nd:YAG. Yan *et al* [56–58] fabricated hollow Pt and Al_2O_3 NPs using a 50 ns pulsed excimer laser for ablating solid Pt and Al targets in water. The authors propose that the hollow nanoparticles are generated at the boundary of bubbles produced by the laser, which provide a nucleation site for self assembly of the laser-fabricated clusters.

Figure 6 shows TEM images of Ni colloidal suspension obtained after fs laser ablation. Microscopy images were performed with a TEM-MSC (JEOL 2100, acceleration voltage 200 KV) at Brazilian Nanotechnology National Laboratory (LNNano). Images of the samples on a single-tilt sample holder were recorded/captured using a TV Gatan ES500W and a CCD (TVips-16MP) camera. Panel (a) is a panoramic view where different spherical structures can be observed, as was predicted by fitting the extinction spectra by OES technique. Panel (b) is another panoramic view where NPs of larger sizes can be observed, coincident with the secondary maxima shown in the inset of figure 5. These large NPs are placed in a different plane with respect to the other agglomerates of NPs. Panel (c) shows an example of air-Ni NP structure, with a size compatible with the size distribution for this structure derived from OES. Finally, panel (d) shows a size histogram of the sample corresponding to panels (a), (b) and (c).

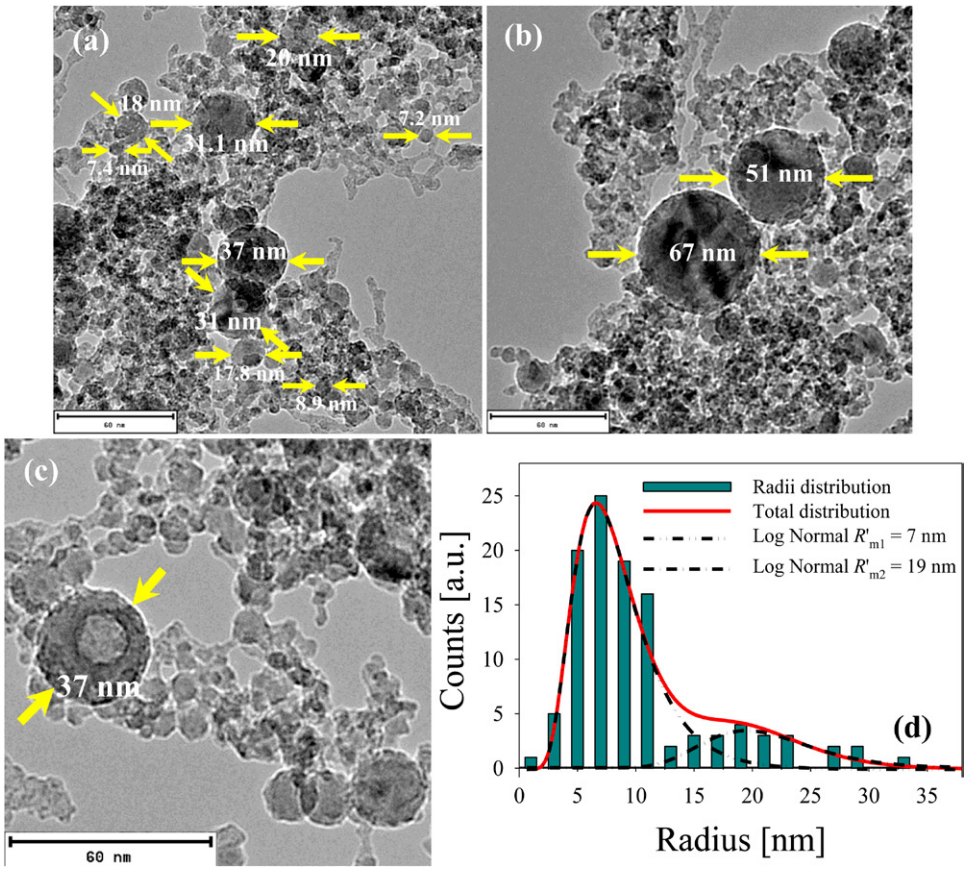

Figure 6. TEM panoramic images of Nps present in Ni colloidal suspension in water showing (a) bare core and core-shell NPs, (b) larger size NPs and (c) air-Ni NPs. (d) Size histogram showing a bimodal distribution. Notice the similarity with size distribution derived from OES distribution in figure 5. Scale bar is 60 nm.

Sizes arising from TEM analysis are in reasonable agreement with results derived from OES shown in figure 5. Spherical bare core and core-shell structures can be observed. This fact supports the use of Mie theory for calculating extinction spectra. Although TEM statistics (10^2–10^3 NPs) is much smaller than OES's (10^{10}–10^{11} NPs), the results of size distribution derived from both techniques are very similar.

4. Conclusions

We have calculated the Drude parameters ω_p and γ_{free} of Ni, Mo, W, Pb, Zn and Na with a new approach based on the value of the slope of linear relations derived from the Drude dielectric function expression as a function of $1 - \varepsilon'(\omega)$ for large wavelengths. This method avoids the often used approximation $\omega \gg \gamma_{free}$, thus improving the precision in its determination. When the values of these parameters are introduced in the expression of the full bulk complex dielectric function, the curves fit very well the full range of experimental data, as compared with the curves calculated using the same parameters given by other authors. The high reliability of the obtained continuous dielectric function renders larger precision in the modelling of bulk optical properties of these metals in an extended wavelength range. This fact is the basis for calculating optical response in the nanometric scale.

For describing the dielectric function of small metal NP in a 'top-down' approach, the classical Drude expression with size correction for the damping constant was rewritten as the sum of the experimental bulk values plus two calculated size corrective terms, one for free electron and the other for bound electron contributions. This new expression for the full complex size-dependent dielectric function has the advantage of uncoupling the experimental and theoretical terms. This is the first time that the dielectric function of the studied metals is calculated for bulk, nanometric and subnanometric structures.

Finally, the optical extinction spectrum of Ni NPs prepared by fs laser ablation method in water was fitted using Mie Theory, taking into account the full expression for the size-dependent dielectric function. From the fitting procedure, a log-normal NPs size distribution including different core-shell species such as Ni-NiO, NiO-Ni and air-Ni is obtained. These results are in reasonable agreement with TEM analysis of the samples.

Acknowledgments

This work was granted by PIP 0280 (CONICET) and 11/I151 (Facultad de Ingeniería, UNLP). We thank C2NANO-Brazilian Nanotechnology National Laboratory (LNNano) at Centro Nacional de Pesquisa em Energia e Materiais (CNPEM)/MCT

(#14825 and 14827) and Research Proposal TEM-16976 for the use of TEM.

D. C. Schinca is Member of Comisión de Investigaciones Científicas de la Provincia de Buenos Aires (CIC). L B. Scaffardi and J M J Santillán are researchers of CONICET. D Muraca is Member of Instituto de Física 'GlebWataghin' (IFGW), Campinas, Brazil. D Muñetón Arboleda and L J Mendoza Herrera are PhD fellows of CONICET, Argentina.

References

[1] Bönnemann H and Richards R M 2001 *Eur. J. Inorg. Chem.* **2001** 2455
[2] Das S K and Marsili E 2011 Bioinspired metal nanoparticle: synthesis, properties and application *Nanomaterials* ed M M Rahman (Croatia: InTech) Chapter 11 pp 253–74
[3] Rodríguez-Llamazares S *et al* 2008 *J. Nanosci. Nanotechnol.* **8** 3820
[4] Cao L, Shu X, Liang D and Wang C 2014 *Spectrosc. Spectral Anal.* **34** 1914
[5] Elango G and Roopan S M 2015 *Spectrochim. Acta* A **139** 367
[6] Huanbuttaa K, Sriamornsak P, Luangtana-anan M, Limmatvapirat S, Puttipipatkhachorn S, Lim L-Y, Terada K and Nunthanid J 2013 *Eur. J. Phar. Sci.* **50** 303
[7] Choi H-J, Choi J-S, Park B-J, Eom J-H, Heo S-Y, Jung M-W, An K-S and Yoon S-G 2014 *Sci. Rep.* **4** 6271
[8] Salema W, Leitnera D R, Zingla F G, Schratterc G, Prasslc R, Goesslerd W, Reidla J and Schild S 2015 *Int. J. Med. Microbiol.* **305** 85
[9] Timilsina U, Singh K P, Tamang H K and Thapa S 2013 *Biomed. Res.* **24** 67–71
[10] Muralisankar T, Bhavan P S, Radhakrishnan S, Seenivasan C, Manickam N and Srinivasan V 2014 *Biol. Trace Elem. Res.* **160** 56
[11] Siddiqui M A *et al* 2015 *Colloids Surf.* B **125** 73
[12] Hdz-García H M, Pech-Canul M I, Muñoz-Arroyo R, Mtz-Enriquez A I, Acevedo-Dávila J L, M J and Reyes-Valdés F A 2015 *J. Mater. Process. Tech.* **215** 1
[13] Taran N Y, Gonchar O M, Lopatko K G, Batsmanova L M, Patyka M V and Volkogon M V 2014 *Nanoscale Res. Lett.* **9** 289
[14] Gokak I B and Taranath T C 2015 *Int. J. Environ. Sci.* **5** 840
[15] Park J *et al* 2005 *Adv. Mater.* **17** 429
[16] Ramírez-Meneses E, Betancourt I, Morales F, Montiel-Palma V, Villanueva-Alvarado C C and Hernández-Rojas M E 2011 *J. Nanopart. Res.* **13** 365
[17] Theivasanthi T and Alagar M 2013 *Phys. Tech. Sci.* **1** 39
[18] Wei X, Wang M-S, Bando Y and Golberg D 2011 *Sci. Technol. Adv. Mater.* **12** 1
[19] Ismail R A, Al-Jawad S M H and Hussein N 2014 *Appl. Phys.* A **117** 1977
[20] Bhaduri B and Verma N 2014 *Chemical Eng. Res. Des.* **92** 1079
[21] Kvítek O, Siegel J, Hnatowicz V and Švorčík V 2013 *J. Nanomater.* **2013** 743684
[22] Bohren C F and Huffman D R 1998 *Absorption and Scattering of Light by Small Particles* (New York: Wiley)
[23] Johnson P B and Christy R W 1972 *Phys. Rev.* B **6** 4370
[24] Kreibig U and von Fragstein C 1969 *Z. Phys.* **224** 307
[25] Norrman S, Andersson T, Granqvist C G and Hunderi O 1977 *Solid State Commun.* **23** 261
[26] Mendoza Herrera L J, Muñetón Arboleda D, Schinca D C and Scaffardi L B 2014 *J. Appl. Phys.* **116** 233105
[27] Fox M 2011 *Optical Properties of Solids* (Oxford: Oxford University Press)
[28] Kittel C 1987 *Quantum theory of solids* (New York: Wiley)
[29] Ordal M A, Bell R J, Alexander R W Jr, Long L L and Querry M R 1987 *Appl. Opt.* **26** 744
[30] Ordal M A, Bell R J, Alexander R W Jr, Newquist L A and Querry M R 1988 *Appl. Opt.* **27** 1203
[31] Rakić A D, Djurišic A B, Elazar J M and Majewski M L 1998 *Appl. Opt.* **37** 5271
[32] Motulevich G. P. and Shubin A. A. 1969 *Sov. Phys. JETP* **29** 24
[33] Inagaki T, Emerson L C, Arakawa E T and Williams M W 1976 *Phys. Rev.* B **13** 2305
[34] Mosteller L P Jr and Wooten F 1968 *Phys. Rev.* **171** 743
[35] Blaber M G, Arnold M D and Ford M J Ford 2009 *Phys. Chem.* C **113** 3041
[36] Brack M 1993 *Rev. Mod. Phys.* **3** 677
[37] Bonacic-Koutecky V, Piercarlo Fantucci J, Koutecky J 1991 *Chem. Rev.* **91** 1035
[38] Scaffardi L B and Tocho J O 2006 *Nanotechnology* **17** 1309
[39] Santillán J M J, Videla F A, Fernández van Raap M B, Schinca D C and Scaffardi L B 2012 *J. Appl. Phys.* **112** 054319
[40] Santillán J M J, Videla F A, Fernández van Raap M B, Muraca D, Scaffardi L B and Schinca D C 2013 *J. Phys. D: Appl. Phys.* **46** 435301
[41] Weaver J H, Lynch D W and Olson C G 1974 *Phys. Rev.* B **1** 501
[42] Golovashkin A I and Motulevich G P 1968 *Sov. Phys. JETP* **26** 881
[43] Lenham A P and Treherne D M 1964 *Proc. Phys. Soc.* **83** 1059
[44] Petrovykh D Y, Altmann K N, Höchst H, Laubscher M, Maat S, Mankey G J and Himpse F J 1998 *App. Phys. Lett.* **73** 3459
[45] Bezuglyi E V, Burma N G, Deineka E Y, Fil V D and Kaufmann H-J 1991 *J. Phys.: Condens. Matter* **3** 7867
[46] Choi D, Moneck M, Liu X, Oh S J, Kagan C R, Coffey K R and Barmak K 2013 *Sci. Rep.* **3** 2591
[47] Ashcroft N W and Mermin N D 1976 *Solid State Physics* (Philadelphia: Saunders College)
[48] Kreibig U and Vollmer M 1995 *Optical Properties of Metal Clusters* (Berlin: Springer)
[49] Santillán J M J, Fernández van Raap M B, Mendoza Zélis P, Coral D, Muraca D, Schinca D C and Scaffardi L B 2015 *J. Nanopart. Res.* **17** 1
[50] Liu B, Hu Z, Che Y, Chen Y and Pan X 2007 *Appl. Phys. Lett.* **90** 044103
[51] Khan S Z, Yuan Y, Abdolvand A, Schmidt M, Crouse P, Li L, Liu Z, Sharp M and Watkins K G 2009 *J. Nanopart. Res.* **11** 1421
[52] Rosensweig R E 2002 *J. Magn. Magn. Mater.* **252** 370
[53] Goya G F, Fonseca F C, Jardim R F, Muccillo R, Carreño N L V, Longo E and Leite E R 2003 *J. Appl. Phys.* **93** 6531
[54] Mahmoud S A, Alshomer S and Tarawnh M A 2011 *J. Mod. Phys.* **2** 1178
[55] Desarkar H S, Kumbhakar P and Mitra A K 2013 *Laser Phys. Lett.* **10** 055903
[56] Yan Z, Bao R and Chrisey D B 2010 *Nanotechnology* **21** 145609
[57] Yan Z, Bao R, Huang Y and Chrisey D B 2010 *J. Phys. Chem.* C **114** 11370
[58] Yan Z, Bao R, Wright R N and Chrisey D B 2010 *Appl. Phys. Lett.* **97** 124106